Energy Advances

ROYAL SOCIETY OF CHEMISTRY

COMMUNICATION

View Article Online
View Journal | View Issue

Cite this: *Energy Adv.*, 2022, 1, 191

Received 20th January 2022,
Accepted 1st March 2022

DOI: 10.1039/d2ya00015f

rsc.li/energy-advances

A localized high concentration electrolyte for 4 V-class potassium metal batteries†

Wenxin Xu,‡ Huwei Wang,‡ Yueteng Gao, Yaojie Wei, Haodong Zhang, Chongwei Gao, Feiyu Kang* and Dengyun Zhai*

Rechargeable potassium-metal batteries (PMBs) meet the need for high energy density because the potassium (K) metal anode has the highest specific capacity (687 mA h g^{-1}) among anode materials, but electrolytes that are stable with both the highly reactive K metal anode and high-voltage cathodes remain a serious challenge. Here, we report a localized high concentration electrolyte consisting of potassium bis(fluoroslufonyl)imide (KFSI) in diethylene glycol dimethyl ether (G2) with 1,1,2,2-tetrafluoro-1-(2,2,2-trifluoroethoxy)-ethane (TFETFE) (1 : 1.5 : 1.5) as a diluent for 4 V-class PMBs. This new electrolyte shows unprecedented cycling stability in K|Prussian blue (PB) batteries with a capacity retention of 83% over 2000 cycles (over 10 months) at a charge cut-off voltage of 4.3 V. Higher voltage tolerance of 4.4 V is also confirmed in the PMBs for 300 cycles. This study provides an avenue to design electrolytes for high-energy PMBs in the future.

Introduction

The development of stationary high-energy energy storage systems is of great significance for regulating the energy output of intermittent energy sources (solar, wind and ocean energy, *etc.*) to achieve social sustainability.[1] Potassium ion batteries (PIBs) can meet the low-cost but high energy density requirements for large-scale energy storage applications due to the high abundance of potassium (K) (2.09 wt%) in the earth's crust and high operating voltage for PIBs.[2] Generally, graphite is the leading anode for PIBs; however, owing to its relatively low theoretical capacity of 279 mA h g^{-1}, the graphite anode cannot guarantee high energy output.[3] In this regard, employing a K metal anode with a higher theoretical capacity of 687 mA h g^{-1} and a low electrochemical potential (−2.93 V *versus* the standard hydrogen electrode) has promising prospects to improve the energy density.[4] Meanwhile, matching high-voltage (normally, 4 V-class) cathode materials is also key to the achievement of high-energy potassium metal batteries (PMBs). However, the development of high-voltage PMBs has been caught in a dilemma because there are very limited reported suitable electrolytes that are stable against both the highly reactive K anode and 4 V-class cathodes.[5,6]

Conventional carbonate electrolytes have been almost exclusively used in PIBs because of their good compatibility with the graphite anode and high oxidative stability (>4.3 V *versus* K^+/K),[3] but their intrinsic reactivity towards highly reactive K metal restricts the Coulombic efficiency (CE) of K plating/stripping to below 50%.[7] To address this serious problem, ether-based electrolytes with good reductive stability have been developed to stabilize the K metal anode and allow long-term reversible K plating/stripping.[7–9] However, the oxidative stability of ethers in regular 1 M salt concentration electrolytes is poor (<4.0 V *versus* K^+/K), prohibiting their applications in 4 V-class PMBs. Note that this has become a common problem of ether electrolytes in alkaline metal (Li, Na, K) batteries.[10] A recent consensus has been reached in the electrolyte research community—increasing the salt concentration.[11] Highly concentrated electrolytes (HCEs) and localized high concentration electrolytes (LHCEs) were therefore developed.[12–15] Because of the enhanced coordination of cations with anions/solvents and the significant reduction of free solvents, these salt-concentrated strategies effectively widen the electrochemical voltage window of the electrolytes.[4,11] Nevertheless, the development of this strategy in K-ion electrolytes is far from ideal. Earlier efforts of Wu *et al.* in potassium bis(fluoroslufonyl)imide (KFSI)/1,2-dimethoxyethane (DME) (mole ratio = 0.6) electrolytes failed to operate PMBs at a cut-off voltage higher than 4.0 V.[7] Although later attempts on HCE formulations (7 mol kg^{-1} KFSI/DME,[16] 5.5 mol kg^{-1} KFSI/DEGDME,[17] and 5 mol L^{-1} KTFSI/DME[18]) succeeded in matching 4 V-class Prussian blue analogue (PBA) cathodes with a cut-off voltage of 4.3 V in PMBs, the unsatisfactory average CEs (~97%)

Shenzhen Geim Graphene Center, Institute of Materials Research, Tsinghua Shenzhen International Graduate School, Tsinghua University, Shenzhen 518055, China. E-mail: fykang@tsinghua.edu.cn, zhaidy0404@sz.tsinghua.edu.cn

† Electronic supplementary information (ESI) available. See DOI: 10.1039/d2ya00015f

‡ These authors contributed equally.

and limited cycle numbers (<350C)[16–18] have highlighted the urgent need to develop suitable electrolytes for 4 V-class PMBs. Moreover, the currently developed HCEs for 4 V-class PMBs inevitably have the problems of high viscosity, poor ion conductivity and high cost. Although a promising K-ion LHCE formulation for the graphite anode has been recently reported, the high-voltage stability of this LHCE has only been tested at a 4 V cut-off voltage.[19] Therefore, the development of a new LHCE formulation based on a suitable low-polarity cosolvent to address all of the above problems will undoubtedly be a breakthrough in K-ion electrolyte design for 4 V-class PMBs.

Herein, a new LHCE formulation consisting of KFSI in diethylene glycol dimethyl ether (G2) with 1,1,2,2-tetrafluoro-1-(2,2,2-trifluoroethoxy)ethane (TFETFE) (1 : 1.5 : 1.5, molar ratio) as a cosolvent was designed. It was demonstrated that the introduction of electrochemically "inert" TFETFE diluent did not change the solvation structure of the original HCE. The obtained LHCE enabled a stable potential window up to 5 V, low viscosity (5.4 mPa S) and high ionic conductivity (6.28 mS cm^{-1}) at the same time. As a result, an unprecedented cycling stability was obtained in a K|Prussian blue (PB) battery at a charge cut-off voltage of 4.3 V (83% capacity retention after 2000 cycles for over 10 months with average CE of 99.7%). More promisingly, stable cycling of PMBs at a higher cut-off voltage (4.4 V) can also be realized in this new LHCE, demonstrating its great potential applications for 4 V-class PMBs.

Results and discussion

A conventional low concentration electrolyte (LCE) consisting of 1 M KFSI in G2 and a HCE consisting of 4.7 M KFSI in G2 were prepared as reference electrolytes, with the KFSI/G2 molar ratio of 1 : 7 and 1 : 1.5, respectively. Here, M stands for molar concentration (mol L^{-1}), *i.e.*, one mole of salt dissolved in a liter of solvent. TFETFE was selected as a cosolvent to construct LHCE (2.3 M KFSI in G2/TFETFE, 1 : 1.5 : 1.5, molar ratio) due to its relatively low solvating power and viscosity. Linear sweep voltammetry (LSV) measurement was first conducted to probe the electrochemical window of the three electrolytes (Fig. 1b). For the LCE, the onset potential starts at ~4.0 V due to the poor oxidation stability of free G2 solvents. In contrast, the onset potentials of both the HCE and LHCE shift positively to almost 5.0 V. Meanwhile, the surface of the Al current collectors in the LCE after electrochemical polarization shows clear corrosion pits, but the pits can be hardly observed in the HCE and LHCE (Fig. S1, ESI†). The common issue of Al corrosion in KFSI-based electrolytes thus can be addressed by employing HCE and LHCE. Furthermore, the cathode compatibility of different electrolytes was verified in K|PB coin cells in a cyclic voltammetry (CV) test (Fig. S2, ESI†).

The long-term cycling performance of K|PB cells in the HCE and LHCE were then investigated with a charge cut-off voltage of 4.3 V. A conventional ester electrolyte formulation of 0.5 M KPF_6 in EC/DEC (1 : 1, volume ratio) was selected as the ester reference electrolyte due to its well-known oxidation stability (>4.3 V) for high-voltage cathodes in PIBs. As shown in Fig. 1a, the K|PB batteries exhibited noticeable differences in cycling stability with different electrolytes. It is clear that the cell with the conventional ester electrolyte showed fast capacity fading, and maintained very low reversible capacity of less than 70 mA h g^{-1} after 340 cycles, suggesting the poor compatibility of the ester electrolyte with the K metal anode, which is consistent with previous observations.[20] When the ether-based HCE was used, the cycling stability of the cell improved greatly with a capacity retention up to 90% after 240 cycles. However, the stable cycles in the HCE were achieved only at a very low current density of 10 mA g^{-1} (Fig. 1a). This is attributed to the high viscosity and poor ion conductivity of the HCE, which will be discussed later. In contrast, the cell with the LHCE exhibited a superior long-term cycling performance with a high capacity retention over 83% after 2000 cycles (only 0.0086% capacity decay per cycle) and an average CE of as high as 99.7% at 50 mA g^{-1}. Note that such a long-term cycling stability (over 10 months) has not been validated previously in 4 V-class PMBs with ether-based electrolytes. Moreover, the voltage polarization of the K|PB cell in the LHCE remained almost unchanged during long-term cycling (Fig. S3c, ESI†),

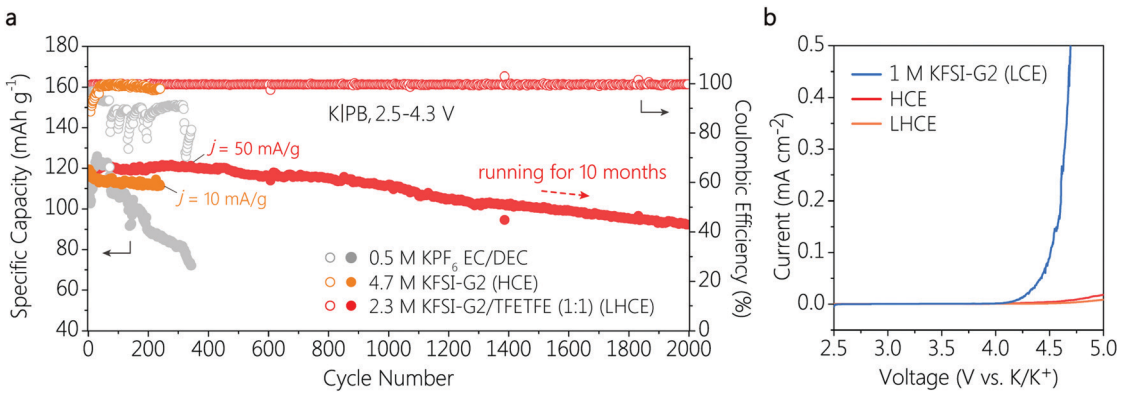

Fig. 1 (a) Cycling performance of K|PB batteries in 0.5 M KPF_6 EC DEC electrolyte at 50 mA g^{-1}, HCE at 10 mA g^{-1}, and LHCE at 50 mA g^{-1}. (b) LSV of various concentrations of KFSI/G2 electrolytes in K|Al coin cells with Al as the working electrode and K metal as the counter electrode. The scan rate is 0.5 mV s^{-1}.

and the high reversibility suggests the formation of an effective solid electrolyte interphase (SEI) on the K anode and stability of the cathode interface.[9] This is further confirmed by observing that a rapidly rising CE in the initial cell cycles can be only achieved in the cell with the LHCE (Fig. S4, ESI†). Although no voltage polarization was observed in the limited cycles of the cell in the HCE (Fig. S3b, ESI†), the CE of K|PB cell only reached 97.4% even after 30 cycles.

Raman measurement was performed to unveil the details of the solvation structures of different electrolytes. As shown in Fig. 2a, free G2 molecules demonstrated vibration peaks at 805 and 852 cm^{-1}. After the addition of the KFSI salt, two new peaks appeared at 838 and 866 cm^{-1} in LCE, HCE and LHCE due to the coordination of G2 molecules to K^+.[21] Note that the vibration peaks of free G2 molecules disappeared entirely in the HCE, indicating that virtually all G2 molecules coordinated to K^+.[22] Meanwhile, with the salt concentration increasing, the vibration peak at 718 cm^{-1} (assigned to the FSI^-) in the LCE shifted to 730 cm^{-1} in the HCE. This observation indicates that concentrated FSI^- anions replace G2 molecules in the K^+ solvation sheath and the FSI^- anions exist in the form of contact ion pairs (CIPs, FSI^- coordinates with one K^+) and aggregates (AGGs, FSI^- coordinates with two or more K^+).[22,23] For the LHCE, except for the presence of the vibration band of TFETFE at 660, 849 and 868 cm^{-1}, it showed peak features similar to that of the HCE, which verifies that the cosolvent TFETFE does not engage in the K^+ solvation structure. As a result, the CIPs and the AGGs solvation structures are well preserved in the LHCE. In this regard, the LHCE undoubtedly inherits the beneficial properties of the HCE including suppressed solvent decomposition and widened voltage window. In addition, the schematic illustration of the solvation structure of LCE, HCE and the diluted LHCE is shown in Fig. 2b.

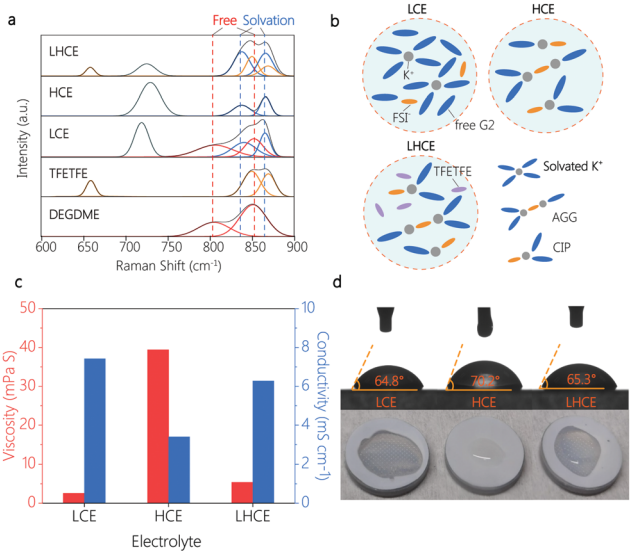

Fig. 2 (a) Raman spectra of LCE, HCE and LHCE. (b) Schematic illustration of the solvation structure of LCE, HCE and the diluted LHCE. (c) Viscosity and ionic conductivity of LCE, HCE and LHCE. (d) Contact angles and wettability tests between the separator and different electrolytes.

Furthermore, the introduction of TFETFE into the HCE also brings favourable physical properties. Specifically, the diluted LHCE showed a much lower viscosity of 5.37 mPa S than the original HCE (39.38 mPa S) (Fig. 2c). The obvious decrease in electrolyte viscosity contributes to the separator wetting. As shown in Fig. 2d, the LHCE exhibited comparable wettability to the LCE, while the HCE droplets were difficult to spread on the separator. These observations are consistent with the results of the contact angle test (Fig. 2d). At the same time, the ionic conductivity of the LHCE increased from 3.4 mS cm^{-1} (HCE) to 6.28 mS cm^{-1}, approaching that of the LCE (Fig. 2c). It is the improved ionic conductivity of the LHCE that ensures the normal operation of the K|PB cells with a current density of 50 mA g^{-1}, but the cells in the HCE suffered from poor reaction kinetics and thus operated under a small current density of 10 mA g^{-1} (Fig. 1a).

Electrochemical impedance spectroscopy (EIS) was conducted to investigate the kinetic properties of the interfacial layer of the K|PB cells with HCE and LHCE. Of particular interest is that the interfacial resistance of the cells with both HCE and LHCE decreased significantly upon cycling (Fig. S5a and b, ESI†), which is probably associated with the formation and gradual stabilization of the interfacial layer on the electrodes. Note that compared with the HCE, a faster resistance decrease can be observed in the LHCE in the initial 10 cycles (Fig. S5c, ESI†), indicating a faster formation of a stable SEI in the LHCE. This phenomenon is consistent with the observation that CE of the K|PB with the LHCE reached more than 99% in the very limited initial cycles (Fig. S4, ESI†). Moreover, the cell using LHCE showed much lower interfacial resistance compared to the cell using HCE (Fig. S5c, ESI†), contributing to the better interfacial reaction kinetics. As a result, a better rate performance of the K|PB cell was achieved in the LHCE (Fig. S4d, ESI†).

To further reveal the difference in the interfacial behavior of different electrolytes, the reversibility of K plating/stripping was evaluated in K|Cu coin cells by galvanostatic cycling tests. As shown in Fig. 3a, the K|Cu cell using the conventional ester electrolyte showed very low CE below 50%, suggesting the poor stability between the ester and the K metal anode, which is consistent with previous observation.[7] In the HCE, the CE greatly increased to 97.9% with a clear charge/discharge overpotential of larger than 400 mV (Fig. 3c). And in the LHCE, a comparable average CE of 98.2% was achieved during 300 cycles for 600 hours. But the overpotential decreased to 300 mV (Fig. 3d), indicating a better electrochemical kinetics compared to that of the HCE. These findings can be attributed to the formation of a stable SEI with lower interfacial resistance in the LHCE, highlighting a good interfacial compatibility between the metallic K anode and the LHCE, and thus enabling highly stable K|PB batteries.

The K metal deposition morphology was carefully studied *via* scanning electron microscopy (SEM). Fig. 3e–j show SEM images of K metal deposited onto the Cu substrate for different electrolytes, at a current density of 0.5 mA cm^{-2} with a capacity of 4.0 mA h cm^{-2}. This high areal capacity allows us to evaluate the compactness of K deposits, considering the "hostless"

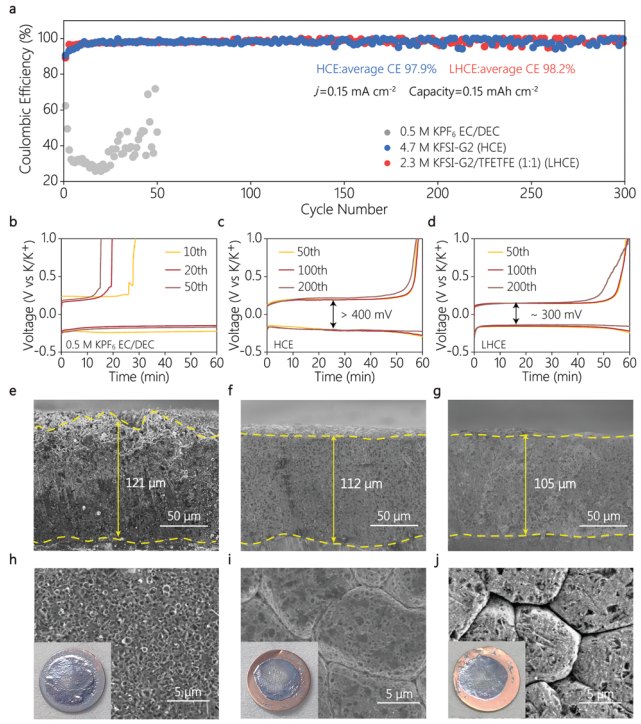

Fig. 3 (a) Cycling performances of K|Cu coin cells and the corresponding voltage profiles in (b) 0.5 M KPF_6 EC/DEC electrolyte, (c) HCE and (d) LHCE at 0.15 mA cm^{-1}. (e–g) Cross-sectional and (h–j) top-view SEM images of K deposition morphologies in (e and h) 0.5 M KPF_6 EC/DEC, (f and i) HCE and (g and j) LHCE. Optical images of K deposits on Cu foil are shown in the inset of h–j. The capacity of K metal on the Cu substrate was 4.0 mA h cm^{-2}.

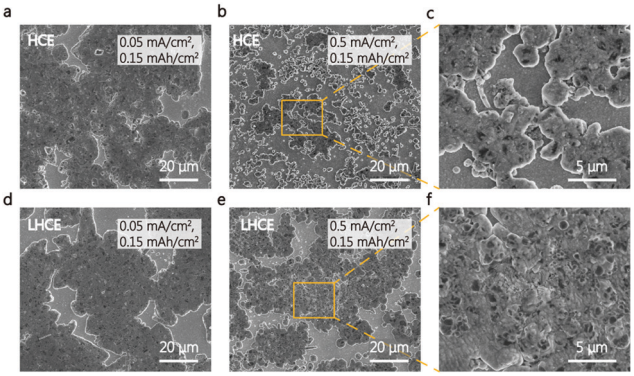

Fig. 4 Top-view SEM images of K deposition morphologies in (a–c) HCE and (d–f) LHCE with enlarged views (c and f) at a current density of (a and d) 0.05 mA cm^{-2} and (b and e) 0.5 mA cm^{-2} with a capacity of 0.15 mA h cm^{-2}.

nature of the metallic K anode.[2,24,25] Irregular and non-dense K deposits were clearly visible in the conventional carbonate electrolyte (Fig. 3e and h). The unstable SEI in ester leads to the thickest K deposits with a coarse surface,[26] which deteriorated the electrochemical performance of the K|Cu and K|PB cells. In contrast, the K metal deposited in the HCE and LHCE showed a similar densely packed and flat morphology (Fig. 3f, g, i, and j). In addition, it is clear that the K deposits in the LHCE were thinner than those in the ester electrolyte (Fig. 3g). As a "hostless" anode, such dense deposition and stable interface suggests the stability of metallic K in the LHCE, which enables the superior cycling stability of the K|PB cells. Furthermore, a low deposition capacity was used to analyse the deposit distribution at a very early deposition state (Fig. 4). At a low current density of 0.05 mA cm^{-2}, no clear morphology differences between HCE and LHCE can be identified, where packed pancake-like K deposits can be seen (Fig. 4a and d). Nevertheless, at a high current density (0.5 mA cm^{-2}), the K deposits in HCE became uneven and non-dense (Fig. 4b and c). In contrast, the K deposits in LHCE maintained densely packed (Fig. 4e and f). Note that the difference is unnoticeable at the large deposition capacity (4 mA h cm^{-2}, Fig. 3), which is consistent with previous observation.[9] Undoubtedly, fast ion diffusion and uniform ion distribution at the interface in LHCE contribute to the formation of the uniform K deposits, further highlighting the superior interfacial reaction kinetics of the LHCE.[19,27–29]

In addition, X-ray photoelectron spectroscopy (XPS) was performed to analyse the chemical compositions of the SEI formed on the K metal anode in different electrolytes. As shown in Fig. S6 and S7 (ESI†), inorganic species of K_2O and KS_xO_y, as well as an abundance of KF were found in the SEI formed in the HCE and LHCE, suggesting that the FSI^- anions in the solvation sheath make a great contribution to the formation of the SEI.[2,8,9] Note that the common SEI components found in both electrolytes support the conclusion that the addition of cosolvent maintains the solvation structure of the HCE. This inorganic-rich SEI is generally believed to facilitate the interfacial ion diffusion[30] and provide sufficient mechanical strength to accommodate the volume change of "hostless" K.[31] Meanwhile, the diluent cosolvent is thought to be beneficial to the formation of a homogeneous SEI,[27] which renders good mechanical stability for accommodating deformation.[32] This may further explain the formation of uniform K deposition in the LHCE during the rapid nucleation stage (Fig. 4e and f). As for the ester, an inorganic-lean but organic-dominated SEI with much oxycarbides can be identified,[25,26] where the apparent enrichment of –C═O– species suggests the continuous decomposition of the ester solvents (Fig. S6a, ESI†). Although the similarity in SEI composition between HCE and LHCE fails to explain the difference in overpotential and interfacial resistance observed in K|Cu and K|PB cells, the great improvement of physical properties of the LHCE cannot be overlooked when regarding the interfacial reaction kinetics.[19,27–29]

Besides the electrolyte stability on the K metal anode, the PMB cycling stability also depends on the stability of the high-voltage cathode. However, this issue remains unexplored in the ether-based electrolytes because very limited reports have addressed high-voltage applications.[16,17] Herein, XPS depth profiling analysis on PB cathodes was carried out to understand the reasons for the cycling stability at a high cut-off voltage of 4.3 V in the HCE and LHCE. Fig. S8 (ESI†) shows the atomic ratio evolution that was calculated based on elementary peak

areas (Fig. S9 and S10, ESI†). A similar trend with close atomic ratios can be observed in the HCE and LHCE. This undoubtedly establishes that the solvation structure dominates the interfacial chemistry on the cathode, which can explain the similarity in the two electrolytes. Specifically, the presence of C–O–K (C 1s spectra, Fig. S9a, ESI† and O 1s spectra, Fig. S10b, ESI†) indicates that a small part of the free solvent is involved in the formation of a surface film on the cathode, which is consistent with previous observations.[14,33] It is noteworthy that the F content gradually increased and remained unchanged with the increasing of the etching time. A similar trend in the peak intensity of KF can be observed in the F 1s spectra (Fig. S9b, ESI†). This phenomenon demonstrates that more KF species are distributed in the inner layer of the surface film on the cathode. The enrichment of inorganic fluoride in the inner layer is believed to contribute to the stability of the cathodes.[33,34]

Furthermore, important merits including low viscosity, high ionic conductivity and good interface stability brought by the LHCE can be best signified when testing PMBs under higher cut-off potentials. Currently, very rare reports have successfully applied ether-based electrolytes with cut-off voltages exceeding 4.3 V in PMBs,[17] which limits the future development of high-voltage cathodes. In this work, we evaluated the K|PB cell performance under a challenging cut-off potential of 4.4 V. As shown in Fig. S11 (ESI†), as expected, the cells with the conventional ester electrolyte exhibited a poor capacity retention (lower than 50%) after 150 cycles as a result of unavoidable degradation of the metallic K anode.[2] When paired with the LHCE, the K|PB cells can be cycled up to 4.4 V with an average CE of 97.9% over 300 cycles. This is unprecedented for PMBs using ether electrolytes, even comparable to the anodic limit of carbonate electrolytes, which highlights the great potential of the LHCE in 4 V-class PMBs.

Conclusions

In summary, we have demonstrated the excellent cyclability of both a high-voltage PB (up to 4.4 V) and the K anode achieved in localized concentrated ether electrolytes. The addition of TFETFE diluent in the HCE contributes to great improvement of its physical properties, including lower viscosity, higher ionic conductivity and better wettability. At the same time, the unchanged FSI^- anion-dominated solvation structure ensures the formation of an inorganic-rich interface, on both sides of the K metal anode and PB cathode. As a result, a highly stable 4 V-class PMB operation for over 10 months can be achieved. Our results demonstrate the advantages of using ether electrolyte for 4 V-class PMBs and provide a better understanding of the LHCE family.

Conflicts of interest

There are no conflicts to declare.

Acknowledgements

This work was supported by the National Natural Science Foundation of China (No. 52072206), Local Innovative and Research Teams Project of Guangdong Pearl River Talents Program (2017BT01N111), and Shenzhen Stable Supporting Project (WDZC20200818155913001).

Notes and references

1 B. Kang and G. Ceder, *Nature*, 2009, **458**, 190–193.
2 H. Wang, D. Zhai and F. Kang, *Energy Environ. Sci.*, 2020, **13**, 4583–4608.
3 J. Wang, H. Wang, X. Zang, D. Zhai and F. Kang, *Batteries Supercaps*, 2021, **4**, 554–570.
4 J. Xiang, L. Yang, L. Yuan, K. Yuan, Y. Zhang, Y. Huang, J. Lin, F. Pan and Y. Huang, *Joule*, 2019, **3**, 2334–2363.
5 M. Zhou, P. Bai, X. Ji, J. Yang, C. Wang and Y. Xu, *Adv. Mater.*, 2021, **33**, 2003741.
6 J. Park, J. Lee, M. H. Alfaruqi, W.-J. Kwak, J. Kim and J.-Y. Hwang, *J. Mater. Chem. A*, 2020, **8**, 16718–16737.
7 N. Xiao, W. D. McCulloch and Y. Wu, *J. Am. Chem. Soc.*, 2017, **139**, 9475–9478.
8 W. Xu, H. Wang, J. Hu, H. Zhang, B. Zhang, F. Kang and D. Zhai, *Chem. Commun.*, 2021, **57**, 1034–1037.
9 H. Wang, J. Dong, Q. Guo, W. Xu, H. Zhang, K. C. Lau, Y. Wei, J. Hu, D. Zhai and F. Kang, *Energy Storage Mater.*, 2021, **42**, 526–532.
10 X. Fan and C. Wang, *Chem. Soc. Rev.*, 2021, **50**, 10486–10566.
11 Y. Yamada, J. Wang, S. Ko, E. Watanabe and A. Yamada, *Nat. Energy*, 2019, **4**, 269–280.
12 J. Qian, W. A. Henderson, W. Xu, P. Bhattacharya, M. Engelhard, O. Borodin and J.-G. Zhang, *Nat. Commun.*, 2015, **6**, 6362.
13 J. Wang, Y. Yamada, K. Sodeyama, C. H. Chiang, Y. Tateyama and A. Yamada, *Nat. Commun.*, 2016, **7**, 12032.
14 X. Cao, X. Ren, L. Zou, M. H. Engelhard, W. Huang, H. Wang, B. E. Matthews, H. Lee, C. Niu and B. W. Arey, *Nat. Energy*, 2019, **4**, 796–805.
15 S. Jiao, X. Ren, R. Cao, M. H. Engelhard, Y. Liu, D. Hu, D. Mei, J. Zheng, W. Zhao and Q. Li, *Nat. Energy*, 2018, **3**, 739–746.
16 T. Hosaka, K. Kubota, H. Kojima and S. Komaba, *Chem. Commun.*, 2018, **54**, 8387–8390.
17 T. Hosaka, T. Matsuyama, K. Kubota, R. Tatara and S. Komaba, *J. Mater. Chem. A*, 2020, **8**, 23766–23771.
18 J. Touja, P. N. Le Pham, N. Louvain, L. Monconduit and L. Stievano, *Chem. Commun.*, 2020, **56**, 14673–14676.
19 L. Qin, N. Xiao, J. F. Zheng, Y. Lei, D. Y. Zhai and Y. Y. Wu, *Adv. Energy Mater.*, 2019, **9**, 1902618.
20 G. He and L. F. Nazar, *ACS Energy Lett.*, 2017, **2**, 1122–1127.
21 P. Geysens, V. S. Rangasamy, S. Thayumanasundaram, K. Robeyns, L. Van Meervelt, J.-P. Locquet, J. Fransaer and K. Binnemans, *J. Phys. Chem. B*, 2018, **122**, 275–289.
22 J. Zheng, S. Chen, W. Zhao, J. Song, M. H. Engelhard and J.-G. Zhang, *ACS Energy Lett.*, 2018, **3**, 315–321.
23 L.-L. Jiang, C. Yan, Y.-X. Yao, W. Cai, J.-Q. Huang and Q. Zhang, *Angew. Chem., Int. Ed.*, 2021, **60**, 3402–3406.

24 L. Qin, Y. Lei, H. Wang, J. Dong, Y. Wu, D. Zhai, F. Kang, Y. Tao and Q.-H. Yang, *Adv. Energy Mater.*, 2019, **9**, 1901427.
25 H. Wang, J. Hu, J. Dong, K. C. Lau, L. Qin, Y. Lei, B. Li, D. Zhai, Y. Wu and F. Kang, *Adv. Energy Mater.*, 2019, **9**, 1902697.
26 J. Hu, H. Wang, S. Wang, Y. Lei, L. Qin, X. Li, D. Zhai, B. Li and F. Kang, *Energy Storage Mater.*, 2021, **36**, 91–98.
27 X. Q. Du and B. A. Zhang, *ACS Nano*, 2021, **15**, 16851–16860.
28 X. Ren, S. Chen, H. Lee, D. Mei, M. H. Engelhard, S. D. Burton, W. Zhao, J. Zheng, Q. Li, M. S. Ding, M. Schroeder, J. Alvarado, K. Xu, Y. S. Meng, J. Liu, J.-G. Zhang and W. Xu, *Chem*, 2018, **4**, 1877–1892.
29 S. Chen, J. Zheng, L. Yu, X. Ren, M. H. Engelhard, C. Niu, H. Lee, W. Xu, J. Xiao, J. Liu and J.-G. Zhang, *Joule*, 2018, **2**, 1548–1558.
30 X.-Q. Zhang, X. Chen, X.-B. Cheng, B.-Q. Li, X. Shen, C. Yan, J.-Q. Huang and Q. Zhang, *Angew. Chem., Int. Ed.*, 2018, **57**, 5301–5305.
31 L. Fan, R. Ma, Q. Zhang, X. Jia and B. Lu, *Angew. Chem., Int. Ed.*, 2019, **58**, 10500–10505.
32 Y. Gao, Z. Hou, R. Zhou, D. Wang, X. Guo, Y. Zhu and B. Zhang, *Adv. Funct. Mater.*, 2022, 2112399.
33 X. Ren, L. Zou, X. Cao, M. H. Engelhard, W. Liu, S. D. Burton, H. Lee, C. Niu, B. E. Matthews, Z. Zhu, C. Wang, B. W. Arey, J. Xiao, J. Liu, J.-G. Zhang and W. Xu, *Joule*, 2019, **3**, 1662–1676.
34 L. Suo, W. Xue, M. Gobet, S. G. Greenbaum, C. Wang, Y. Chen, W. Yang, Y. Li and J. Li, *Proc. Natl. Acad. Sci. U. S. A.*, 2018, **115**, 1156–1161.